RSC Advances

ROYAL SOCIETY OF CHEMISTRY

www.rsc.org/advances

RSC Advances

ARTICLE

Visible Light Assisted Photocatalytic Hydrogen Generation by Ta_2O_5/Bi_2O_3, $TaON/Bi_2O_3$, and Ta_3N_5/Bi_2O_3 Composites†

Received 00th January 20xx,
Accepted 00th January 20xx

DOI: 10.1039/x0xx00000x

www.rsc.org/

Shiba P. Adhikari,[a, b] Zachary D. Hood,[c] Karren L. More,[c] Ilia Ivanov,[c] Lifeng Zhang,[d] Michael Gross,[a, b] and Abdou Lachgar*[a, b]

Composites comprised of two semiconducting materials with suitable band gaps and band positions have been reported to be effective at enhancing photocatalytic activity in the visible light region of the electromagnetic spectrum. Here, we report the synthesis, complete structural and physical characterizations, and photocatalytic performance of a series of semiconducting oxide composites. UV light active tantalum oxide (Ta_2O_5) and visible light active tantalum oxynitride (TaON) and tantalum nitride (Ta_3N_5) were synthesized, and their composites with Bi_2O_3 were prepared *in situ* using benzyl alcohol as solvent. The composite prepared using equimolar amounts of Bi_2O_3 and Ta_2O_5 leads to the formation of the ternary oxide, bismuth tantalate ($BiTaO_4$) upon calcination at 1000 ^{0}C. The composites and single phase bismuth tantalate formed were characterized by powder X-ray diffraction (PXRD), thermogravimetric analysis (TGA), Brunauer-Emmett-Teller (BET) surface area measurement, scanning electron microscopy (SEM), transmission electron microscopy (TEM), UV-Vis diffuse reflectance spectroscopy, and photoluminescence. The photocatalytic activities of the catalysts were evaluated for generation of hydrogen using aqueous methanol solution under visible light irradiation ($\lambda \geq 420$ nm). The results show that as-prepared composite photocatalysts extend light absorption range and restrict photogenerated charge-carrier recombination, resulting in enhanced photocatalytic activity compared to individual phases. The mechanism for the enhanced photocatalytic activity for the heterostructured composites is elucidated based on observed activity, band positions calculations, and photoluminescence data.

1. Introduction

After the discovery of titanium dioxide (TiO_2) as an ultraviolet light active photocatalyst for water splitting and degradation of organic compounds in the early 1970's, a large number of semiconductor-based photocatalysts have been extensively studied.[1,2] In a semiconductor photocatalytic system, electron-hole pairs are generated when a photocatalyst is exposed to light with energy larger than that of its band gap ($h\nu \geq E_g$). The photogenerated electron-hole pairs can either recombine with no chemical effect or migrate to the surface of the semiconductor without recombination, where they can be effectively used to carry out specific redox processes.[3,4] Thus, the efficacy of the photocatalytic process depends on *(i)* the number of charge carriers taking part in the redox reactions and *(ii)* the effective separation of electron hole pairs generated by the photoexcitation. High recombination, (i.e. short lifetime of the photo-generated carriers) and limited efficiency under visible light are the two limiting factors in the development of efficient semiconductor-based photocatalysts.

A number of metal oxides and sulfides have been examined as photocatalysts for hydrogen production and decomposition of toxic organic molecules.[5,6] The majority of binary and ternary semiconducting metal oxides (e.g. TiO_2, $NaTaO_3$) are primarily active under UV irradiation, which represents only 5% of solar spectrum. For better utilization of solar energy, the materials should have band gaps less than 3 eV ($\lambda > 385$ nm).[7] Thus, significant efforts have been invested in the development of new or modified semiconductor photocatalysts capable of being active in the visible region of the electromagnetic spectrum (λ= 400–700 nm).[8–10] The most common approach is the use of cation and/or anion doping to engineer band gaps of UV-active semiconducting oxides by extending their absorption range to better utilize visible light.[3,11–13] Despite the success of this chemically-based strategy, the performance of visible light active doped photocatalysts remains relatively low in comparison to that of UV active photocatalysts. For example, K. Nagaveni *et al*. has compared the photocatalytic activities of different metal ion (W, V, Ce, Zr, Fe, and Cu) doped and undoped TiO_2 and their results showed that the degradation rates of 4-nitrophenol with doped catalysts were lower than that of the undoped TiO_2 both with UV exposure and solar radiation.[14] The

[a] Department of Chemistry, Wake Forest University, Winston-Salem, NC 27109, USA, E-mail: lachgar@wfu.edu; Fax: +1-336-758-4656; Tel: +1-336-758-4676
[b] Center for Energy, Environment and Sustainability, Wake Forest University, Winston-Salem, NC 27109, USA
[c] Center for Nanophase Materials Sciences (CNMS), Oak Ridge National Laboratory (ORNL), Oak Ridge, TN, 37831
[d] Joint School of Nanoscience and Nanoengineering, North Carolina A&T State University, 2907 East Lee Street, Greensboro, NC 27401, USA

†Electronic Supplementary Information (ESI) available: [Synthesis, XRD of tantalum oxide and BITA composite before calcination (Fig. 1S), SEM and EDS spectrum (Fig. 2S), TEM images (Fig. 3S), UV/Vis diffuse reflectance spectra of synthesized products (Fig. 4S), TGA study of BITA composite, Ta_2O_5 and Bi_2O_3 (Fig. 5S), Nitrogen Adsorption desorption isotherms (Fig. 6S)]. See DOI: 10.1039/b000000x/

other approach that has generally been applied is to form a semiconductor heterojunction by coupling with a secondary substance (either a dye or another semiconductor).[15–20] This approach was examined in a variety of applications including hydrogen generation and organic molecule degradation. Some studies focused on the enhancement of visible light induced activity of high band gap semiconductors (UV light active) by combining it with small band gap semiconductors (visible light active).[16–18] Other studies used composite photocatalysts made of two or more small band gap semiconductors (both visible light active).[19,20] In general, it is believed that properly designed heterostructured systems (composite photocatalysis) help to separate photogenerated electron-hole pairs, thus increasing the pairs' life time so that they can transfer to the surface to participate in redox processes. Taking into account the above mentioned facts of charge carrier recombination and absorption range extension, we synthesized, characterized, and studied photocatalytic properties of visible light active composite photocatalysts prepared from two semiconducting oxides with suitable band gaps and band positions.

Among the semiconductor oxides, tantalum-based materials attract considerable attention in the field of photocatalytic hydrogen generation because of its unique chemical stability as well as excellent electronic characteristics for water splitting. The conduction band (CB) levels consist of tantalum 5d orbital (more negative than the Titanium 3d orbital), which gives photogenerated electrons a strong reducing capability. However, practical use of Ta_2O_5 as a photocatalyst is limited because of its activity is restricted to UV light as well as its low photocatalytic activity. Many studies focused on improving catalytic activity of Ta_2O_5 by preparing large surface area materials, doping with cations or anions and making composites with other catalysts.[21–24] Another important semiconducting oxide, bismuth oxide, has recently captured considerable attention due to its visible light activity, dielectric permittivity, high refractive index, and thermal stability.[25] It is a semiconductor with suitable band positions for water oxidation.[26] It has also been proven to be an excellent sensitizer to enhance visible light activity of UV or visible active photocatalysts. The approach involving the fabrication of heterostructured composites using bismuth oxide as a sensitizer have been successful in reducing the photogenerated charge carrier recombination and optical response extension.[16,27–30] A number of bismuth oxide based heterojunctions, such as $Bi_2O_3/BaTiO_3$,[16] ZnO/Bi_2O_3,[25] and $Bi_2O_3/TiO_{2-x}N_x$,[29] have shown excellent photocatalytic activity when exposed to visible light. Here, we report the synthesis of new semiconducting heterojunctions formed by combining tantalum oxides, nitrides, and oxynitrides with bismuth oxide. These composites show superior photocatalytic activities compared to pure tantalum oxide, tantalum oxynitride and tantalum nitride for generation of hydrogen gas in an aqueous solution of methanol using visible light. The enhanced mechanisms of the photocatalytic activity of these heterojunctions are rationalized on the basis of corresponding band gaps, band positions and photoluminescence data. In the case of heterojunction formed of bismuth oxide and tantalum oxide, an equimolar ratio of the two oxides was used to study the photocatalytic activity of composites as well as that of the bismuth tantalate phase ($BiTaO_4$) which is obtained after calcination. $BiTaO_4$ is a well-known photocatalyst suitable for overall water splitting as well as organic molecule degradation.[31–33] This paper details how bismuth oxide may be used to create composites with tantalum-based simple oxides, oxynitrides and nitrides. The heterojunction between the two components is characterized and discussed in detail.

2. Experimental Section

2.1 Synthesis

2.1.1 Synthesis of Bi_2O_3/ Ta_2O_5 composite

For the synthesis of the Bi_2O_3/Ta_2O_5 composite, bismuth nitrate pentahydrate ($Bi(NO_3)_3.5H_2O$, Alfa Aesar, 99 %) and tantalum chloride ($TaCl_5$, Alfa Aesar, 99.9% metals basis) were used as received. A two-step synthesis approach was used to obtain the composite. In the first step, Ta_2O_5 nanoparticles were prepared using anhydrous benzyl alcohol as solvent.[34] In the second step, the as-prepared Ta_2O_5 nanoparticles were used as a support during the synthesis of bismuth oxide using bismuth nitrate precursor in benzyl alcohol under reflux conditions. Detailed synthesis of Ta_2O_5 nanoparticles is given in supplementary information. In a typical synthesis of the composite, 0.5 g of Ta_2O_5 nanoparticles were transferred to a 100 mL round bottom flask along with 50 ml of anhydrous benzyl alcohol. Then, 1.097 g bismuth nitrate pentahydrate (to make equimolar ratio of bismuth oxide and tantalum oxide) was added to this suspension and refluxed at 150 °C for 8 hours with continuous magnetic stirring. The obtained pale yellow product was washed with ethanol and vacuum dried for 12 hours at 70 °C. The product was then calcined at 400 °C to obtain the Bi_2O_3/ Ta_2O_5 composite, BITA-400, as determined by PXRD. The yield of BITA-400 was ~ 80 %, based upon the weight of bismuth oxide and tantalum oxide. A sample of the product was also calcined at 1000 °C to obtain the phase BiTaO4 (BITA-1000) as confirmed by PXRD.

2.1.2 Synthesis of Bi_2O_3/ TaON and Bi_2O_3/ T_3N_5 composites

To better understand the behaviour of these heterostructured composite, two other composites based on tantalum oxynitride (TaON) and tantalum nitride (Ta_3N_5) with bismuth oxide were prepared using the same two-step method described earlier. TaON and Ta_3N_5, were prepared by nitridation of tantalum oxide in ammonia.[35,36] The complete synthesis procedure is described in the supporting information. The surface of TaON and Ta_3N_5 are coated with Bi_2O_3 using the reflux method as described above and calcined at 400 °C for 2 hours to obtain composites of Bi_2O_3/TaON (BITON) and Bi_2O_3/Ta_3N_5 (BITN) respectively.

2.2 Characterization

The products were characterized by powder X-ray diffraction (PXRD) using a Bruker-D8, with Cu-Kα radiation (λ=0.15418 nm). The morphology and EDAX analysis of the samples were determined by scanning electron microscopy using an SEM, JSM-6380-LA, JEOL, Japan) and transmission electron microscopy (TEM, JEOL JEM2010). The morphologies and structures of the obtained composites were further analysed by a scanning transmission electron microscope (STEM, JEOL 2200-FS) with aberration corrected at 200 kV. Differential scanning calorimetry (DSC) and thermogravimetric analysis (TGA) were completed using an SDT-Q600 (TA instrument, USA) from 32-1000 °C under constant airflow

and a heating rate of 10 °C/min. The Brunauer-Emmett-Teller (BET) surface areas were determined from nitrogen adsorption isotherms at 77 K using Autosorb-iQ from Quantachrome. UV-vis diffuse reflectance spectra (DRS) were collected on a Shimadzu UV-3600 spectrophotometer equipped with an integrating sphere. Photoluminescence (PL) spectra were measured on the dual grating Fluorometer-3T (JY Horiba), with right angle configuration of excitation and detection. The excitation was made with 300 nm monochromatic light, with slits on the excitation and detection monochromators set at 5 nm.

2.3 Photocatalytic test

The catalysts were evaluated for their photocatalytic hydrogen generation using 20 % (v:v) aqueous solution of methanol under visible light ($\lambda \geq 420$ nm) and UV + visible light irradiation. A 300 W Xenon lamp (Newport Corporation) was used as the light source with a 420 nm cut-off filter to provide visible light irradiation. All experiments were performed at ambient temperature (25 °C) using a water jacket around the photocatalytic cell. In a typical reaction, 50 mg of the as-prepared photocatalyst was dispersed in an aqueous solution of methanol (10 mL of methanol and 40 mL of deionized water). Before illumination, the suspension was degassed using argon gas for 30 min in order to remove any dissolved oxygen. Then, the solution was exposed to visible or UV light irradiation under magnetic stirring. The amount of hydrogen produced was quantified by gas chromatography.

3. Results and discussion

3.1 Characterization of photocatalysts

The crystal structures and phases of the samples studied were investigated by powder X-ray diffraction (PXRD), as shown in Fig. 1. The PXRD pattern of BITA-400 composite (Fig. 1a) confirms the formation of pure tetragonal bismuth oxide (JCPDS- 074-1371) and tantalum oxide (JCPDS- 079-1375). Similarly, patterns of BITON (Fig. 1b) and BITN (Fig. 1c) show the composite formation of TaON (JCPDS-071-0178) and Ta_3N_5 (JCPDS-089-5200) phases, respectively, with Bi_2O_3 (JCPDS-079-1375). The major peaks in Fig. 1a, 1b and 1c (located at about 2θ = 28.12°, 32.9°, 46.3°, 47.0° and 55.7°) correspond to the tetragonal phase of Bi_2O_3. The other major reflections in Fig. 1a correspond to the orthorhombic phase of Ta_2O_5. The broadening of peaks in Fig. 1a suggests small crystallite size. Using the Scherrer equation, the average crystallite sizes of Bi_2O_3 and Ta_2O_5 are estimated to be 26 nm and 32 nm, respectively. Similarly the crystallite size of TaON and Ta_3N_5 in BITON and BITN are calculated to be 55 nm and 52 nm, respectively. The peaks in Fig. 1b observed at 2θ = 18.11°, 29.5° and 32.0° correspond to the monoclinic form of TaON.[35,36] Besides the peaks of bismuth oxide, major peaks in Fig. 1c correspond to the monoclinic phase of Ta_3N_5. The PXRD shown in Fig. 1d correspond to that of the pure $BiTaO_4$ (JCPDS- 016-0909) obtained after the calcination of BITA composite at 1000 °C.

Based on the PXRD study, it is confirmed that the crystal structure representation of the individual components of the composites studied differ from each other substantially (Table 1). Ta_2O_5 is orthorhombic while TaON and Ta_3N_5 are monoclinic. These tantalum based compounds are coated with the tetragonal phase of Bi_2O_3 during their composite formation. These individual components of the composite are well known photocatalysts for solar fuel production and light initiated environmental remediation processes. [37–39]

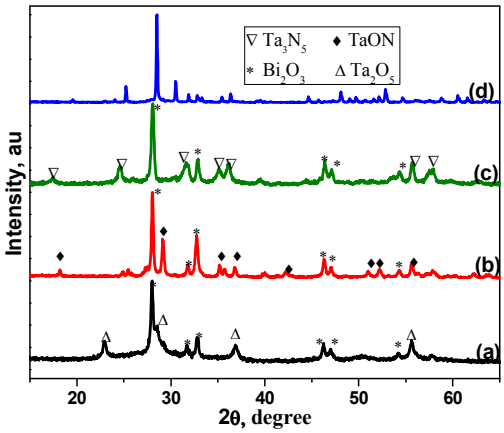

Fig. 1 - PXRD Patterns of the samples (a) BITA-400, (b) BITON, (c) BITN and (d) BITA-1000 ($BiTaO_4$).

Table 1 - Crystal structure representation, and electronic structure data of the components of the composites studied. These composites are made with tetragonal Bi_2O_3 and different phases of tantalum based compounds (orthorhombic Ta_2O_5 for BITA-400 composite, monoclinic TaON for BITON composite and monoclinic Ta_3N_5 for BITN composites).

Compounds		Ta_2O_5	TaON	Ta_3N_5	Bi_2O_3
Crystal unit cell representation		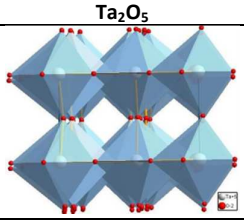	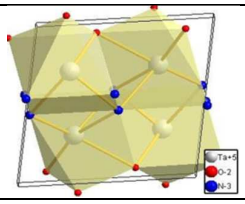	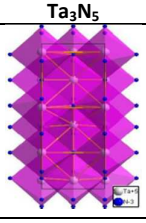	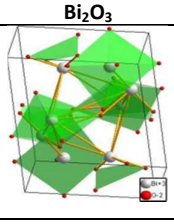
Color of sample		White	Yellow-green	Red	Yellow
Band Gap, eV		3.80	2.29	2.03	2.78
Calculated band Positions, eV vs NHE	CB	-0.17	-0.17	-0.17	+0.34
	VB	+3.63	+2.12	+1.86	+3.11

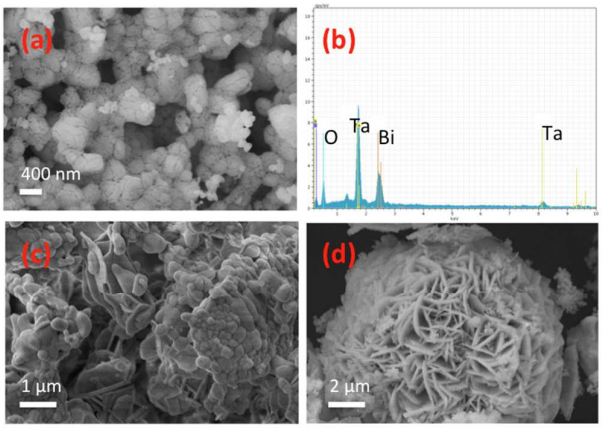

Fig. 2 - SEM images and EDS spectrum for different samples: (a) and (b) BITA-400, (c) BITON, (d) BITN.

The morphology and microstructure of different samples were revealed by scanning electron microscopy (SEM) and scanning tunnelling electron microscopy (STEM) as shown in Fig. 2 and 3. Additional microscopy images of composites studied can be found in the supporting information (Fig. 2S and Fig. 3S). The composites are composed of irregular architectures with micron sized particles. Energy dispersion spectroscopy (EDS) of BITA-400 shows the presence of Bi and Ta only (Fig. 2b). The composites were further analysed by scanning tunnelling electron microscope (STEM) to understand the nature of the heterojunctions. As shown in Fig. 3a and b, the BITA-400 composite consists of block-like Ta_2O_5 nanosize particles with well-defined faces, whereas Bi_2O_3 particles tend to be primarily acicular or spherical shape. Elemental mapping (Fig. 3b), clearly shows that the Bi_2O_3 and Ta_2O_5 phases are segregated from each other with no intimate contact. In contrast, the composite BITON consists of nanosize block-like or cuboidal TaON particles (~50 nm in size) intimately combined with Bi_2O_3 particles of similar size to form larger porous particles. The elemental mapping shown on fig. 3d demonstrate the intimate nature of the BITON composite. Similar conclusion is true for the composite BITN. SEM image (fig 2d) shows the formation of onion-shaped micron-size particles formed of plate-like crystals. STEM images and elemental mapping shown in Fig 3e and 3f indicate formation of intimate mixture of the two individual phases.

The optical absorption properties of all samples were measured by UV–vis absorption spectra transformed from the corresponding diffuse spectra according to the Kubelka–Munk theory and the results are shown in Fig. 4S (supporting info).[40,41] The band gaps obtained from UV-vis diffuse reflectance spectra were used to calculate the position of the conduction band (CB) bottom (E_{CB}) using the empirical formula:[42]

$$E_{CB} = X - 0.5\,E_g + E_0 \qquad (1)$$

where E_g is the band gap energy of the semiconductor, E_0 is a scale factor relating the reference electrode redox level to absolute vacuum scale (E_0 = −4.5 eV for normal hydrogen electrode, NHE), and X is the electronegativity of the semiconductor, which can be expressed as the geometric mean of the absolute electronegativity of the constituent atoms.[43] The values of E_{CB} and E_{VB} calculated by using this empirical formula are consistent with the reported values.[44]

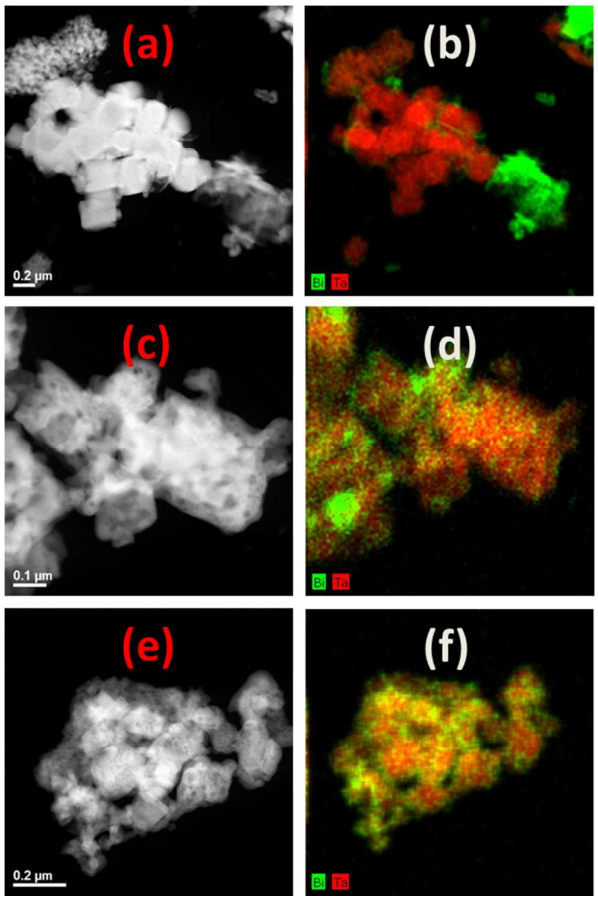

Fig. 3 - STEM images of (a) BITA-400, (c) BITON, (e) BITN composites with corresponding mapping analysis (b), (d) and (f).

The DSC-TGA curves of BITA composite are presented in Fig. 4. The first weight loss begins at ~175 °C, and corresponds to the loss of organics used during synthesis. The loss of organics is complete by ~400 °C. The weight was almost constant after 400 °C. This is supported by the major exothermic peak in DSC curve as well. Hence, this temperature was used to calcine all synthesized Bi_2O_3 based composites to remove all organic molecules in order to obtain the pure phase of bismuth oxide in all composites. The pure bismuth tantalate phase was obtained after heating at 1000 °C. Additional TGA graphs of composites and individual component are included in the supporting information (Fig. 5S). To understand the phase changes that occur during the heating of the composites, we collected PXRD data of the phases obtained at various temperatures (Fig. 5). The PXRD shown in Fig. 5a corresponds to that of crystalline Ta_2O_5 used as precursor mixed with amorphous Bi_2O_3. After heating at 400 °C, diffraction peaks of both Ta_2O_5 and Bi_2O_3 are present indicating the initiation of the crystallization of Bi_2O_3 and formation of the composite

BITA-400 (Fig. 5b). When the compound was heated at higher temperatures, crystalline $BiTaO_4$ began to form at temperatures as low as 800 °C. Pure $BiTaO_4$ is obtained at 1000 °C as shown in Fig. 5h.

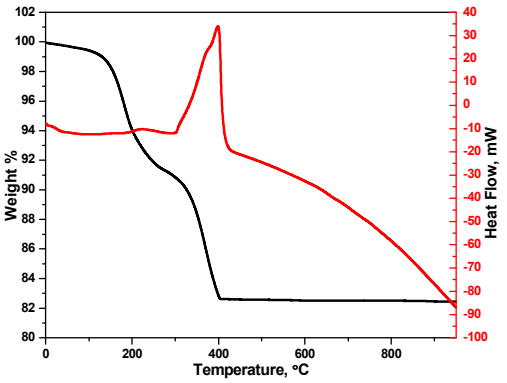

Fig. 4 - DSC-TGA analysis of bismuth oxide and tantalum oxide composite.

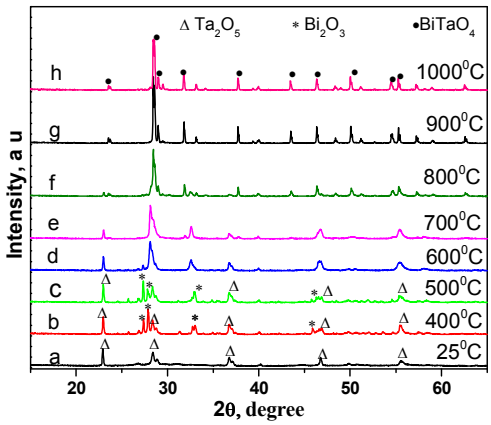

Fig. 5 - XRD study of BITA composite (Bi_2O_3/Ta_2O_5) heated at different temperatures.

Surface area analysis of the samples are summarized in Table 2 and the adsorption/desorption isotherms are shown in Fig. 6S in the supporting information. The surface area of BITA-400 is higher than that obtained for BITON and the BITN. The smaller particles from BITA-400 are further supported by PXRD and SEM results. This is most likely due to the corresponding tantalum oxynitride and tantalum nitride used during the synthesis of the composites. The oxynitride and nitride compounds were prepared by heating tantalum oxide at 825 °C for 6 hours. This calcination may have increased the particle size and reduced the surface area.

3.2 Photocatalytic Testing

The photocatalytic activities of the samples were determined by the amount of hydrogen generated from an aqueous solution of methanol under visible light or UV light irradiation. Fig. 6 and Table 2 display the different amount of hydrogen produced in 4 hours of UV or visible light irradiation by the given samples.

Table 2 - Amount of hydrogen evolved from different catalysts with different surface areas in 4 hours of visible light irradiation.

Photocatalyst	Surface area (m^2/g)	Visible light irradiated H_2 evolution after 4 hour photolysis (μmol/g)
BITA-400	25.00	0.5
TaON	2.50	3
Ta_3N_5	2.05	7
BITON	6.04	68
BITN	5.41	92

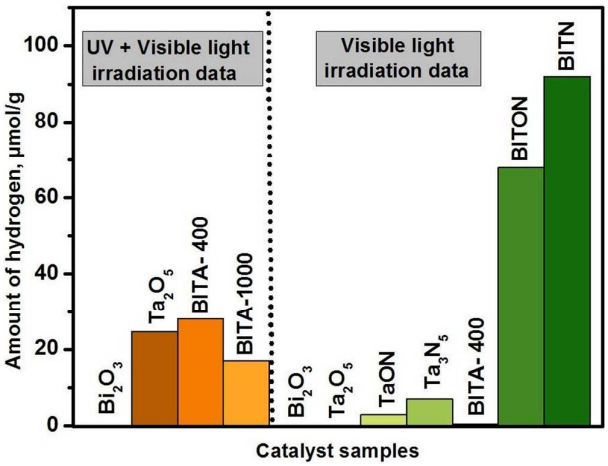

Fig. 6 - Amount of hydrogen gas evolved for different samples in 4 hours (50 mg of catalyst in 50 mL of 20 % aqueous methanol solution irradiated with visible light or UV + visible light).

Since tantalum oxide and bismuth tantalate do not absorb in the visible light region, there was no hydrogen production when only visible light was used. Furthermore, no hydrogen production was observed when bismuth oxide was used alone because its band position is not suitable for water reduction. The UV light activity of the composite BITA-400 was slightly higher than that of tantalum oxide and the ternary BITA-1000. Only a very small amount of hydrogen was observed when BITA-400 was exposed to visible light irradiation. The photocatalytic hydrogen evolution is significant in composite in comparison to the individual components or phase pure samples. In other words, the composites BITON and BITN display significantly better photocatalytic hydrogen production compared to the individual components of the composites.

It was found that, the visible light activated hydrogen evolution rate is found in the order of BITN > BITON > Ta_3N_5 > TaON > BITA-400, suggesting lower recombination rate of photogenerated carriers in the composites. The higher activity of the composites is presumably due to the intimate contact between bismuth oxide and TaON or Ta_3N_5. The intimate contact between particles of the two composite components allows the photo-generated electrons and holes to reside in two different species and restrict their recombination rate. To understand the lifetime of

photogenerated electron hole pairs, we have conducted photoluminescence (PL) for all samples. PL data (Fig. 7) shows that the PL emission intensity (the main emission peak is centred at about 390 nm) is in the order of BITA-1000 > Ta_2O_5 > BITA-400 > TaON > Ta_3N_5 > BITON > BITN. The emission intensity of the PL spectra for the composites is significantly smaller than that of the individual components. The intensity of the PL spectra is directly proportional to the rate of charge carrier recombination.[45–47] The data suggest that there is significantly less recombination in the composites, which may explain the higher photocatalytic activity observed. Thus, formation of composites has led to better separation of photo-generated electrons and holes, increasing the life time of the electron-hole pairs, which enhances the photocatalytic activity.

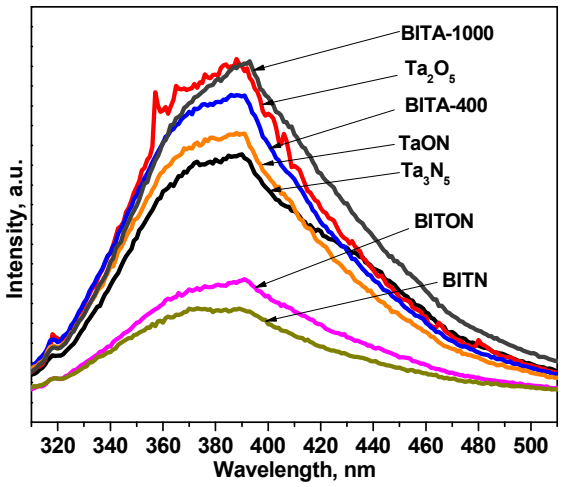

Fig. 7- Room temperature photoluminescence (PL) spectrum of as prepared samples (λ_{Ex} = 300 nm).

3.3 Reaction mechanism

To explain the mechanism of enhanced photocatalytic hydrogen generation for the heterostructured composites, we investigated the relative band positions of two semiconductors because the band edge potentials play a crucial role in determining the flowchart of photo-excited charge carriers in heterojunctions. Fig. 8 shows a schematic representation of band positions of different compounds based on calculated band edges given in Table 1. The band positions of bismuth oxide lay between those of tantalum oxide. Additionally, its valence band position is located below that of TaON and Ta_3N_5.

The activities of the composites are directly related to the corresponding band positons of the individual components. The low activity of the BITA-400 composite (in visible and UV light) can be explained using the same facts observed in the ZrO_2/TaON system, as described by K Maeda *et al.*[48] Based on the band positons of bismuth oxide and tantalum oxide, electron transfer from the conduction band of Bi_2O_3 to the conduction band of Ta_2O_5 and transfer of holes from the valence band of Bi_2O_3 to the valence band of Ta_2O_5 should be energetically unfavourable, and the band positions of bismuth oxide are not suitable for hydrogen generation. Hence, it can be concluded that the electrochemical reactions occur at the surface of tantalum oxide and the incorporation of bismuth oxide helps to separate the electrons and holes on the surface, leading to better activity than the individual tantalum oxide. The increased activity of tantalum oxide over single phase bismuth tantalate (BITA-1000) (Fig. 6) can be explained on the basis of surface area. The surface areas of tantalum oxide and bismuth tantalate are 5.8 m^2/g and 2.05 m^2/g, respectively. The higher surface area brings not only increased surface for contact with transmitted UV light and water molecules for reduction, but also more active catalytic sites. On the other hand, for randomly generated charge carriers, the average diffusion time from bulk to the surface is given by $\tau = r^2/\pi^2 D$, where r is the grain radius and D is the diffusion coefficient of the carrier.[49] When the grain radius decreases, diffusion time is reduced, and the recombination probability of photo-generated electron-hole pairs decreases.

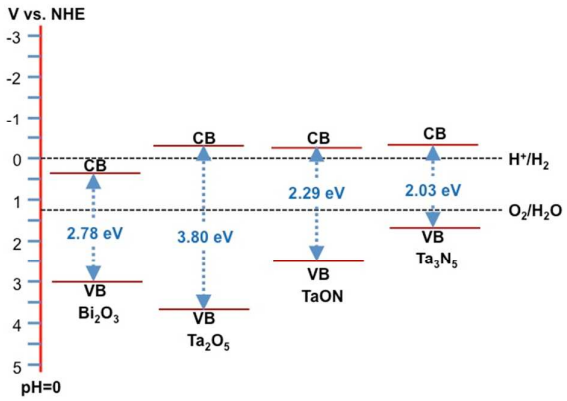

Fig. 8 - Relative band positions of Bi_2O_3, Ta_2O_5, TaON, and Ta_3N_5.

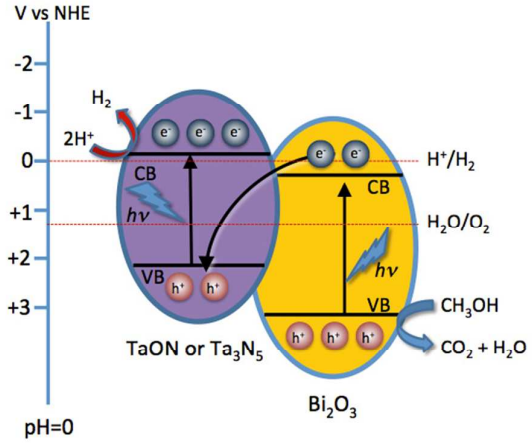

Fig. 9 - Comparative band edge positons and charge transfer process (Z-Scheme) in bismuth oxide and tantalum oxynitride or tantalum nitride heterojunction under visible light irradiation.

The increased visible light activity of the other two composites, namely BITON and BITN (when compared to tantalum oxynitride and tantalum nitride, respectively) can be explained by the trapping of holes due to the presence of bismuth oxide. Under visible light irradiation, both components of each composite become excited, creating electrons and holes in the conduction band and valence band respectively. In principle, it would be expected that electrons from the CB of TaON or Ta_3N_5 would be easily injected in the CB of Bi_2O_3. If electron migration follows this pathway, more electrons would be concentrated in the CB of Bi_2O_3. Based on band position calculations, electrons in the CB of Bi_2O_3 would not be able to reduce protons due to higher positive CB potential in comparison to H^+/H_2 potential. However, for BITN and BITON composites, H_2 evolution is considerably higher than that of individual Ta_3N_5 or TaON. This result implies that electrons in the CB of Ta_3N_5 or TaON in composite BITN or BITON are responsible for hydrogen generation and the corresponding holes are trapped by the CB electrons of Bi_2O_3, similar to the Z-Scheme mechanism as shown in Fig-9.[15,50–53] This mechanism is further supported by the observed higher activity of BITN compared to BITON. The valence band of TaON lies below that of the valence band of Ta_3N_5, thence trapping of holes in VB of Ta_3N_5 by electrons moving from Bi_2O_3 (Z-scheme) is more energetically favourable than the same process in case of TaON. The significant decrease in PL intensity for BITON and BITN composites (Fig. 7) clearly suggest and support the conclusion that the recombination rate of photo-generated electron-hole pairs in TaON or Ta3N5 is significantly reduced when combined with Bi2O3. In all cases, the enhanced activity of heterojunctioned composites containing Bi_2O_3 with tantalum-based simple oxides, oxynitrides and nitrides can be attributed to better electron hole pair separation.

Conclusions

In summary, tantalum oxide, tantalum oxynitride and tantalum nitride based composites were prepared individually using bismuth oxide. The heterojunctions formed between the two components in each catalyst show favourable conditions for electron-hole separation to generate hydrogen from an aqueous methanol solution. On the basis of the calculated energy band positions, the mechanisms of enhanced photocatalytic activity for the composites were discussed; the enhanced activity is attributed to the effective separation of electron hole pairs due to the formation of heterojunctions between the two semiconductors, which allows for better photocatalytic activity for the production of hydrogen gas via water splitting under visible light irradiation.

Acknowledgements

A portion of this research was completed as part of a user proposal through ORNL's Center for Nanophase Materials Sciences (CNMS), which is a DOE Office of Science User Facility. Zachary D. Hood was supported by Higher Education Research Experiences (HERE) at Oak Ridge National Laboratory. The authors would like to thank Ms. Nacole King from North Carolina State University, Raleigh, NC for her support regarding diffuse reflectance spectra. Dr. Cynthia Day from Wake Forest University, Department of Chemistry, is acknowledged for temperature-dependent PXRD data collection. Support from Phase II Triad Interuniversity Project (TIP) is also acknowledged. Support from the WFU Science Research Fund is acknowledged.

Notes and references

1 A. Fujishima and K. Honda, *Nature*, 1972, **238**, 37–38.
2 K. Maeda, *J. Photochem. Photobiol. C Photochem. Rev.*, 2011, **12**, 237–268.
3 M. Ni, M. K. H. Leung, D. Y. C. Leung and K. Sumathy, *Renew. Sustain. Energy Rev.*, 2007, **11**, 401–425.
4 A. Kudo and Y. Miseki, *Chem Soc Rev*, 2009, **38**, 253–278.
5 F. E. Osterloh, *Chem Soc Rev*, 2013, **42**, 2294–2320.
6 A. O. Ibhadon and P. Fitzpatrick, *Catalysts*, 2013, **3**, 189–218.
7 R. Abe, *J. Photochem. Photobiol. C Photochem. Rev.*, 2010, **11**, 179–209.
8 R. Asahi, T. Morikawa, T. Ohwaki, K. Aoki and Y. Taga, *Science*, 2001, **293**, 269–271.
9 M. Tahir and N. S. Amin, *Energy Convers. Manag.*, 2013, **76**, 194–214.
10 C.-H. Liao, C.-W. Huang and J. C. S. Wu, *Catalysts*, 2012, **2**, 490–516.
11 R. Asahi, T. Morikawa, H. Irie and T. Ohwaki, *Chem. Rev.*, 2014, **114**, 9824–9852.
12 P. Kanhere and Z. Chen, *Molecules*, 2014, **19**, 19995–20022.
13 M. Pelaez, N. T. Nolan, S. C. Pillai, M. K. Seery, P. Falaras, A. G. Kontos, P. S. M. Dunlop, J. W. J. Hamilton, J. A. Byrne, K. O'Shea, M. H. Entezari and D. D. Dionysiou, *Appl. Catal. B Environ.*, 2012, **125**, 331–349.
14 K. Nagaveni, M. S. Hegde and G. Madras, *J. Phys. Chem. B*, 2004, **108**, 20204–20212.
15 H. Wang, L. Zhang, Z. Chen, J. Hu, S. Li, Z. Wang, J. Liu and X. Wang, *Chem Soc Rev*, 2014, **43**, 5234–5244.
16 X. Lin, J. Xing, W. Wang, Z. Shan, F. Xu and F. Huang, *J. Phys. Chem. C*, 2007, **111**, 18288–18293.
17 J. S. Jang, H. G. Kim, U. A. Joshi, J. W. Jang and J. S. Lee, *Int. J. Hydrog. Energy*, 2008, **33**, 5975–5980.
18 S. Y. Chai, Y. J. Kim, M. H. Jung, A. K. Chakraborty, D. Jung and W. I. Lee, *J. Catal.*, 2009, **262**, 144–149.
19 M.-S. Gui, W.-D. Zhang, Q.-X. Su and C.-H. Chen, *J. Solid State Chem.*, 2011, **184**, 1977–1982.
20 Z. Zhang, W. Wang, L. Wang and S. Sun, *ACS Appl. Mater. Interfaces*, 2012, **4**, 593–597.
21 M. Sharma, D. Das, A. Baruah, A. Jain and A. K. Ganguli, *Langmuir*, 2014, **30**, 3199–3208.
22 M. Higashi, K. Domen and R. Abe, *J. Am. Chem. Soc.*, 2012, **134**, 6968–6971.
23 M.-Y. Tsang, N. E. Pridmore, L. J. Gillie, Y.-H. Chou, R. Brydson and R. E. Douthwaite, *Adv. Mater.*, 2012, **24**, 3406–3409.
24 R. Abe, M. Higashi and K. Domen, *J. Am. Chem. Soc.*, 2010, **132**, 11828–11829.
25 A. Hameed, V. Gombac, T. Montini, L. Felisari and P. Fornasiero, *Chem. Phys. Lett.*, 2009, **483**, 254–261.
26 M. Li, F. Li and P. G. Yin, *Chem. Phys. Lett.*, 2014, **601**, 92–97.
27 J. XU, M. CHEN and D. FU, *Trans. Nonferrous Met. Soc. China*, 2011, **21**, 340–345.
28 X. Liu, L. Pan, T. Lv, Z. Sun and C. Q. Sun, *J. Colloid Interface Sci.*, 2013, **408**, 145–150.
29 B. Naik, S. Martha and K. M. Parida, *Int. J. Hydrog. Energy*, 2011, **36**, 2794–2802.
30 J. Zhang, Y. Hu, X. Jiang, S. Chen, S. Meng and X. Fu, *J. Hazard. Mater.*, 2014, **280**, 713–722.

31 Z. Zou, J. Ye, K. Sayama and H. Arakawa, *Chem. Phys. Lett.*, 2001, **343**, 303–308.
32 B. Muktha, J. Darriet, G. Madras and T. N. Guru Row, *J. Solid State Chem.*, 2006, **179**, 3919–3925.
33 R. Shi, J. Lin, Y. Wang, J. Xu and Y. Zhu, *J. Phys. Chem. C*, 2010, **114**, 6472–6477.
34 J. Buha, D. Arcon, M. Niederberger and I. Djerdj, *Phys Chem Chem Phys*, 2010, **12**, 15537–15543.
35 T. Takata, G. Hitoki, J. N. Kondo, M. Hara, H. Kobayashi and K. Domen, *Res. Chem. Intermed.*, 2007, **33**, 13–25.
36 W. R. Matizamhuka, I. Sigalas and M. Herrmann, *Ceram. Int.*, 2008, **34**, 1481–1486.
37 Z. Xu, I. Tabata, K. Hirogaki, K. Hisada, T. Wang, S. Wang and T. Hori, *Catal Sci Technol*, 2011, **1**, 397–400.
38 M. Hara, G. Hitoki, T. Takata, J. N. Kondo, H. Kobayashi and K. Domen, *4th Int. Symp. Group Five Compd. Bicenten. Meet.*, 2003, **78**, 555–560.
39 C. M. Fang, E. Orhan, G. A. de Wijs, H. T. Hintzen, R. A. de Groot, R. Marchand, J.-Y. Saillard and G. de With, *J Mater Chem*, 2001, **11**, 1248–1252.
40 G. Burgeth and H. Kisch, *Coord. Chem. Rev.*, 2002, **230**, 41 – 47.
41 H. Lin, C. P. Huang, W. Li, C. Ni, S. I. Shah and Y.-H. Tseng, *Appl. Catal. B Environ.*, 2006, **68**, 1 – 11.
42 H. Cheng, B. Huang, Y. Dai, X. Qin and X. Zhang, *Langmuir*, 2010, **26**, 6618–6624.
43 Y. Xu and M. A. A. Schoonen, *Am. Mineral.*, 2000, **85**, 543–556.
44 W.-J. Chun, A. Ishikawa, H. Fujisawa, T. Takata, J. N. Kondo, M. Hara, M. Kawai, Y. Matsumoto and K. Domen, *J. Phys. Chem. B*, 2003, **107**, 1798–1803.
45 J. Tang, Z. Zou and J. Ye, *J. Phys. Chem. B*, 2003, **107**, 14265–14269.
46 Y. Du, L. Zhao and Y. Zhang, *J. Hazard. Mater.*, 2014, **267**, 55–61.
47 M. T. Mayer, C. Du and D. Wang, *J. Am. Chem. Soc.*, 2012, **134**, 12406–12409.
48 K. Maeda, H. Terashima, K. Kase, M. Higashi, M. Tabata and K. Domen, *Bull. Chem. Soc. Jpn.*, 2008, **81**, 927–937.
49 A. Hagfeldt and M. Graetzel, *Chem. Rev.*, 1995, **95**, 49–68.
50 C.-C. Hu, J.-N. Nian and H. Teng, *Sol. ENERGY Mater. Sol. CELLS*, 2008, **92**, 1071–1076.
51 C. Shifu, J. Lei, T. Wenming and F. Xianliang, *Dalton Trans*, 2013, **42**, 10759–10768.
52 H. Katsumata, Y. Tachi, T. Suzuki and S. Kaneco, *RSC Adv*, 2014, **4**, 21405–21409.
53 K. Kailasam, A. Fischer, G. Zhang, J. Zhang, M. Schwarze, M. Schröder, X. Wang, R. Schomäcker and A. Thomas, *ChemSusChem*, 2015, **8**, 1404–1410.

Table of content:

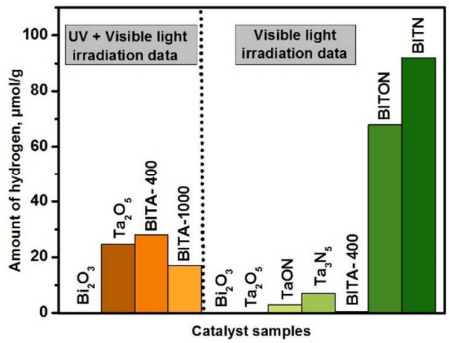

Bi_2O_3/TaON or Ta_3N_5 Heterojunctions show significant enhancement in photocatalytic H_2 production under visible light irradiation compared to individual components.